01,15

Sink strengths of low-angle tilt boundaries for self-point defects in BCC iron and vanadium

© A.B. Sivak[1], V.M. Chernov[2]

[1] National Research Center „Kurchatov Institute“,
Moscow, Russia
[2] A.A. Bochvar Advanced Research Institute for Inorganic Materials,
Moscow, Russia

E-mail: Sivak_AB@nrcki.ru

Received June 4, 2024
Revised June 4, 2024
Accepted June 6, 2024

For low-angle tilt boundaries formed by dislocation walls of straight edge dislocations in slip systems $\langle 111\rangle\{110\}$ and $\langle 111\rangle\{112\}$, the sink strengths for self-point defects (vacancies and self-interstitial atoms) and the bias factors (relative difference in the sink strengths for self-interstitial atoms and vacancies) have been calculated in BCC metals Fe and V. The calculations have been performed using the object kinetic Monte Carlo method in the temperature range 293−1000 K, the subgrain misorientation angles 1.5−10° and the subgrain sizes 150−900 a (a is the lattice parameter). The elastic interaction of self-point defects in stable and saddle-point configurations (elastic dipoles) with the elastic fields of dislocation walls has been calculated by means of the anisotropic theory of elasticity (metals Fe and V differ significantly in the elastic anisotropy ratio). The sink strengths of low-angle boundaries do not depend (within the calculation accuracy) on their type (the slip system of dislocations). The bias factor value varies with temperature in the range of 15−30% and is inversely proportional to the misorientation angle and the size of the subgrains. The bias factors in Fe and V are significantly different (for V it is several times less).

Keywords: low-angle tilt boundaries, sink strengths, bias factors, iron, vanadium.

DOI: 10.61011/PSS.2024.07.58984.147

1. Introduction

Fields of internal stresses in metals have significant effect on formation and kinetics of self-point defects (SPDs: vacancies and interstitial atoms), determining additional (as compared with their absence) features of formation and decomposition of their solid solutions under thermal and radiation exposures. Dislocations and dislocation clusters are main sources of internal stresses in metals [1,2]. The processes determining the radiation properties of metals (swelling, strengthening, creep, and fracture) develop in a system „dislocation cluster — SPDs“. These processes depend on symmetry of crystal lattices, elastic anisotropy of metals and types of formed in them structural defects [1,2]. Due to this it seems important to study the effect of stress fields from dislocations and dislocation clusters (including, low-angle tilt boundaries) on their sink strengths for SPDs in metals with different elastic anisotropy factors. Results of such processes study form the basis for further construction and development of models of formation and evolution of microstructure (formation and mobility of dislocations) and properties (heat resistance, swelling, creep, etc.) of metals under external effects of different nature (radiation, thermal, mechanical) and intensity.

History of theoretical and model calculations of sink strengths of low-angle boundaries and their bias factor (relative difference of sink strengths for self-interstitial atoms (SIAs) and vacancies) counts for more than four decades [3–6]. But in [3–6] interaction between low-angle boundaries and SPDs is considered using isotropic models for medium and SPDs (SPD is considered as a spherical inclusion into isotropic media), but actual metals are elastically anisotropic with specific types and slip systems of dislocations. SPDs symmetry differs from spherical (e.g., elastic dipoles, corresponding to saddle-point configurations of an SIA and a vacancy in BCC crystals Fe and V, have monoclinic and trigonal symmetry, respectively [7]).

The body centered cubic (BCC) metal crystals Fe and V are of important scientific and practical interest, they are basis for development of structural steels and alloys for nuclear and thermonuclear energy reactors. In this study we consider the dislocation clusters in form of low-angle tilt boundaries (LATBs — dislocation walls consisting of straight edge dislocations in basic slip systems $\langle 111\rangle\{110\}$ and $\langle 111\rangle\{112\}$) in BCC crystals Fe and V. The elastic fields of such LATBs and their effect on the formation and direction of SPDs migration were studied by the methods of anisotropic theory of elasticity earlier [7]. The sink strengths of LATBs for SPDs are calculated using an object kinetic Monte Carlo method (OKMC method) considering both elastic anisotropy of studied metals Fe and V, and symmetry of stable and saddle-point configurations of SPDs in these

metals. Based on obtained grid of numerical values of sink strengths of LATBs with discrete set of values of model parameters (temperature ranges 293−1000 K, disorientation angles of subgrains 1.5−10°, subgrain sizes 150−900 a, a — lattice parameter) the analytical expressions are prepared. They ensure calculation of sink strengths of LATBs for arbitrary values of parameters in the specified ranges.

2. Method of calculation of sink strengths of LATBs

The sink strengths of LATBs for SPDs were determined by the OKMC method used previously to determine the sink strengths of spatially uniform networks of dislocations of different types [8–10]. Elastic interaction between LATBs and SPDs, considered as elastic dipoles (a vacancy and a self-interstitial atom in stable and saddle-point configurations), was calculated in the framework of the anisotropic linear theory of elasticity [7]. The interaction of an SPD with only two nearest dislocation walls was considered, as the interaction with other dislocation walls was low to have significant effect on the calculation results. In OKMC calculations at all the temperatures the elastic fields of LATBs were calculated using the values of elastic constants for temperatures close to absolute zero [11,12], since test calculations at the highest temperature considered (1000 K) showed that taking into account the temperature dependence of elastic constants (elastic anisotropy) leads to insignificant change in sink strengths by maximum 3%, and their relative difference for SIAs and vacancies (bias factor) — maximum by 1%.

The schematic image of the simulation cell is shown in Figure 1. The simulation cell was a right-angle prism with rectangular base, along central axis of which one of wall dislocations is located. Periodic boundary conditions (PBC) were imposed on the side faces of the prism. Side lengths of the rectangular base, L_x and L_y, were selected to obtain required distances between neighboring LATBs and subgrain misorientation angle Θ respectively ($\Theta = 2\,\mathrm{arctg}[b/(2h)] \approx b/h$, b is the modulus of the Burgers vector of dislocations ($\mathbf{b}$ along axis x), h the distance between dislocations in the wall, $h = L_y$). L_x was selected equal to 150, 300, 600, 900 a, a is the lattice parameter. L_y was selected equal to $L_y = 33$, 16,5, 10, $5a$, which corresponds to misorientation angles $\Theta = 1.5$, 3.0, 5.0, 10°.

The sink strength of LATB k^2 was determined via the diffusion length of SPDs before their absorption at wall dislocations k^{-1} ($k^2 = 6/(\langle N\rangle\lambda^2)$, where $\langle N\rangle$ is the average number of jumps performed by SPDs from their formation till absorption at sink, $\lambda^2 = 3a^2/4$ the square of SPD jump length in BCC-lattice). It was assumed that an SPD was absorbed by a wall dislocation upon its approach to the dislocation by distance lower than value $r_0 = 3a$. Such value of r_0 was selected following [10], where it had been shown that selection of values r_0, lower than $3a$, had no significant effect on calculated values k^2, since field interaction between SPDs and dislocations made determining contribution to the value k^2. For convenience, the dimensionless value of the sink efficiency of wall dislocations (or LATB dislocations) will also be discussed, it is defined as

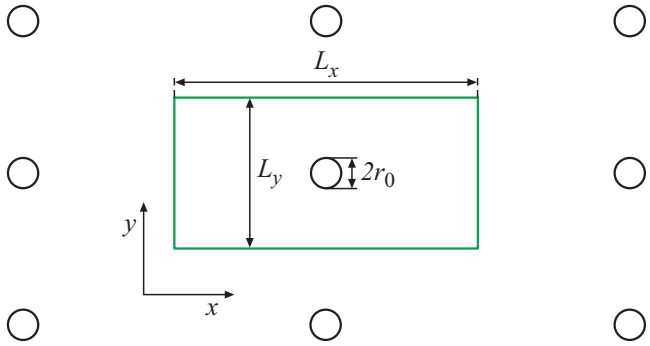

Figure 1. Schematic image of the simulation cell for OKMC calculations of sink strengths of LATBs, consisting of set of parallel dislocations (absorbing cylinders with radius r_0). Rectangle is the simulation cell. Dislocations outside calculation cell are images formed by PBC.

$$\xi = k^2/\rho_\mathrm{d} = k^2 L_x L_y, \tag{1}$$

where ρ_d is the density of LATB-dislocations in crystal.

For each type of SPD and LATB, 10^5 trajectories were simulated, this ensured level of relative accidental error 1% (confidential probability 99%).

The sink strengths and efficiencies of LATB dislocations not considering interaction between LATBs and SPDs were also calculated. They are designated as k_0^2 and ξ_0, respectively. In such calculations r_0 varied in the range $1-10a$, L_y — in the range $5-66a$, L_x — in the range $150-900a$. For each type of SPD and LATB, 10^6 trajectories were simulated, this ensured the level of relative accidental error 0.3% (confidential probability 99%).

3. Results

Results of OKMC simulation show that values of sink strengths of LATBs, consisting of dislocations in slip systems $\langle 111\rangle\{110\}$ and $\langle 111\rangle\{112\}$, coincide within calculation inaccuracy. Further there are results only for the LATB, consisting of dislocations $\langle 111\rangle\{110\}$. Tables 1, 2 list calculated values of sink efficiencies of LATB dislocations $\langle 111\rangle\{110\}$ for SIAs (ξ^+) and vacancies (ξ^-) for BCC crystals Fe, V, respectively, and calculated by them values of LATB bias factors ($D = 1 - \xi^-/\xi^+$) are given in Table 3. Values of sink efficiencies of LATBs not considering their elastic interaction with SPDs are given in Table 4. From the data in Table 3 it is clear that the value D:

1) varies with temperature within the range 15−30%;

Table 1. Sink efficiencies of LATB dislocations in Fe

Θ	T, K	$L_x = 150a$		$L_x = 300a$		$L_x = 600a$		$L_x = 900a$	
		ξ^+	ξ^-	ξ^+	ξ^-	ξ^+	ξ^-	ξ^+	ξ^-
1.5°	293	5.67	2.84	1.93	1.39	0.796	0.678	0.498	0.449
	400	4.92	2.59	1.80	1.32	0.771	0.661	0.488	0.440
	600	4.12	2.36	1.66	1.25	0.742	0.643	0.476	0.432
	800	3.64	2.25	1.57	1.22	0.720	0.635	0.466	0.428
	1000	3.34	2.19	1.50	1.20	0.707	0.629	0.459	0.426
3.0°	293	2.21	1.62	0.845	0.734	0.373	0.349	0.238	0.228
	400	2.08	1.54	0.823	0.713	0.368	0.342	0.236	0.226
	600	1.91	1.44	0.792	0.693	0.361	0.339	0.234	0.224
	800	1.80	1.41	0.771	0.681	0.356	0.336	0.232	0.222
	1000	1.72	1.38	0.755	0.675	0.353	0.334	0.230	0.222
5.0°	293	1.13	0.975	0.473	0.442	0.217	0.210	0.141	0.138
	400	1.10	0.939	0.469	0.434	0.216	0.209	0.141	0.137
	600	1.06	0.906	0.459	0.426	0.214	0.207	0.140	0.136
	800	1.02	0.889	0.452	0.422	0.213	0.206	0.139	0.136
	1000	1.00	0.880	0.447	0.420	0.211	0.205	0.139	0.136
10°	293	0.479	0.461	0.219	0.214	0.105	0.103	0.0686	0.0682
	400	0.476	0.454	0.218	0.213	0.104	0.103	0.0686	0.0680
	600	0.471	0.448	0.217	0.212	0.104	0.103	0.0685	0.0679
	800	0.467	0.447	0.216	0.211	0.104	0.103	0.0684	0.0678
	1000	0.462	0.445	0.215	0.211	0.104	0.103	0.0682	0.0679

Table 2. Sink efficiencies of LATB dislocations in V

Θ	T, K	$L_x = 150a$		$L_x = 300a$		$L_x = 600a$		$L_x = 900a$	
		ξ^+	ξ^-	ξ^+	ξ^-	ξ^+	ξ^-	ξ^+	ξ^-
1.5°	293	3.90	3.17	1.61	1.46	0.730	0.695	0.470	0.457
	400	3.55	2.85	1.54	1.38	0.712	0.677	0.463	0.447
	600	3.13	2.53	1.45	1.30	0.693	0.656	0.454	0.438
	800	2.87	2.37	1.38	1.25	0.678	0.643	0.448	0.432
	1000	2.68	2.28	1.34	1.22	0.667	0.636	0.443	0.429
3.0°	293	1.77	1.65	0.763	0.738	0.354	0.348	0.231	0.228
	400	1.70	1.57	0.746	0.719	0.351	0.345	0.229	0.227
	600	1.60	1.48	0.727	0.698	0.347	0.340	0.228	0.225
	800	1.54	1.42	0.714	0.686	0.343	0.338	0.226	0.223
	1000	1.49	1.40	0.704	0.681	0.341	0.335	0.225	0.222
5.0°	293	0.992	0.957	0.445	0.437	0.211	0.209	0.138	0.137
	400	0.967	0.933	0.440	0.433	0.209	0.208	0.137	0.137
	600	0.937	0.905	0.433	0.425	0.209	0.207	0.137	0.136
	800	0.918	0.890	0.428	0.423	0.207	0.205	0.136	0.136
	1000	0.904	0.882	0.424	0.421	0.207	0.205	0.136	0.135
10°	293	0.455	0.452	0.214	0.212	0.103	0.103	0.0681	0.0682
	400	0.451	0.448	0.213	0.212	0.103	0.103	0.0680	0.0680
	600	0.447	0.445	0.211	0.211	0.103	0.103	0.0679	0.0679
	800	0.446	0.443	0.211	0.211	0.103	0.103	0.0678	0.0676
	1000	0.444	0.443	0.211	0.210	0.103	0.102	0.0679	0.0678

2) is approximately directly proportional to the distance between dislocations in the wall L_y (respectively, inversely proportional to the subgrain misorientation angle Θ);

3) is approximately inversely proportional to the subgrain size L_x;

4) all other things being equal, is several times lower for V than for Fe.

Low negative values D ($|D| < 1\%$) for the LATB with $\Theta = 10°$ in V (Table 3) are due to random error of its determination.

4. Analytical expressions for sink strengths of LATBs not considering interaction of LATBs with SPDs

The sink strength of two parallel planes limiting the material is described as [13]

$$k_0^2 = 12d^{-2} \tag{2}$$

where d is the distance between absorbing planes. Then for plain grains with width W and thickness of grain boundaries δ_0 we can write

$$k_0^2 = 12\,\frac{1+f_V}{(W-\delta_0)^2} = \frac{12}{W^2}\,\frac{1+\delta_0 W^{-1}}{(1-\delta_0 W^{-1})^2}, \tag{3}$$

where $f_V = \delta_0 W^{-1}$ is the volume fraction of sinks in crystal. Multiplier in numerator $(1 + f_V)$ occurs due to the fact that SPDs are generated, among other regions of the crystallite, inside the grain boundary. Comparison of formula (3) with OKMC calculations for such configuration of sinks (Figure 2) showed their full compliance within accuracy of OKMC calculations (inaccuracy below 0.1% at confidential probability 99%) at $W = 150a$ and $\delta_0 = 6a$.

If a boundary consists of absorbing cylinders with radius r_0 (Figure 1), the distance between which is $L_y \le 2r_0$, then

$$k_0^2 \approx 12\,\frac{1+f_V}{(L_x-\overline{\delta}_0)^2} = \frac{12}{L_x^2}\,\frac{1-\overline{\delta}_0 L_x^{-1}}{(1-\overline{\delta}_0 L_x^{-1})^2}, \tag{4}$$

where $\overline{\delta}_0$ is the average width of boundary,

$$\overline{\delta}_0 = r_0\left(\sqrt{1-\varepsilon^2} + \varepsilon^{-1}\arcsin\varepsilon\right), \quad \varepsilon = L_y/2r_0. \tag{5}$$

Table 3. LATB bias factor (in %) in Fe and V

Θ	T, K	$L_x = 150a$		$L_x = 300a$		$L_x = 600a$		$L_x = 900a$	
		Fe	V	Fe	V	Fe	V	Fe	V
1.5°	293	49.8	18.8	28.0	9.2	14.9	4.8	9.8	2.8
	400	47.2	19.7	26.8	10.1	14.3	4.8	9.8	3.4
	600	42.7	19.2	24.7	10.3	13.3	5.4	9.1	3.6
	800	38.2	17.3	22.1	9.4	11.8	5.2	8.1	3.6
	1000	34.3	15.0	20.0	8.6	10.9	4.6	7.1	3.1
3.0°	293	26.5	6.8	13.1	3.4	6.6	1.7	4.2	1.2
	400	26.0	7.5	13.4	3.7	7.0	1.7	4.5	1.2
	600	24.5	7.8	12.5	4.0	6.2	1.9	4.4	1.3
	800	22.0	7.4	11.6	4.0	5.8	1.6	4.1	1.1
	1000	19.9	6.4	10.6	3.2	5.3	1.6	3.6	1.1
5.0°	293	13.8	3.6	6.6	1.7	3.2	0.9	2.4	0.4
	400	14.7	3.5	7.3	1.5	3.3	0.6	2.8	0.2
	600	14.4	3.4	7.3	1.7	3.5	0.9	2.5	0.7
	800	13.1	3.1	6.8	1.3	3.4	0.7	2.4	0.4
	1000	12.1	2.5	6.0	0.8	2.8	0.9	2.1	0.4
10°	293	3.8	0.7	2.0	0.7	1.2	0.0	0.6	−0.1
	400	4.6	0.6	2.1	0.5	1.0	0.0	0.8	0.0
	600	4.9	0.4	2.0	0.3	1.3	−0.2	0.9	0.0
	800	4.3	0.5	2.3	0.1	0.6	0.0	0.9	0.3
	1000	3.8	0.2	2.1	0.3	0.9	0.5	0.4	0.1

At $\varepsilon = 0$ Eq. (4) transforms to Eq. (3) with $\delta_0 = 2r_0$. At $\varepsilon = 1$ ($L_y = 2r_0$), $\overline{\delta}_0 = \pi r_0/2$.

Further for convenience we transfer from expressions for k_0^2 to expressions for ξ_0 ($\xi_0 = k_0^2 L_x L_y$). Since $\overline{\delta}_0 \ll L_x$ at considered ranges of values of model parameters, Eq. (4) can be simplified

$$\xi_0 \approx 12 L_y L_x^{-1}(1 + 3\overline{\delta}_0 L_x^{-1}). \tag{6}$$

Comparison of calculation using Eq. (6) and OKMC calculations for sinks configuration shown in Figure 1, with $L_y = 5a$ and $r_0 = 3a$, showed their good compliance (difference below 0.2%).

At $\varepsilon > 1$ ($L_y > 2r_0$), the value $\overline{\delta}_0$ becomes complex. In this case, the approximating analytical expression can be obtained by choosing such an analytical form that, while L_y tends to $2r_0$, would transit into Eq. (6), and upon L_y tendency to L_x would transit into known expression for absorbing cylinders uniformly distributed in space [14]:

$$\xi_0 = 2\pi(\ln \rho^{-1} - 3/4)^{-1}, \tag{7}$$

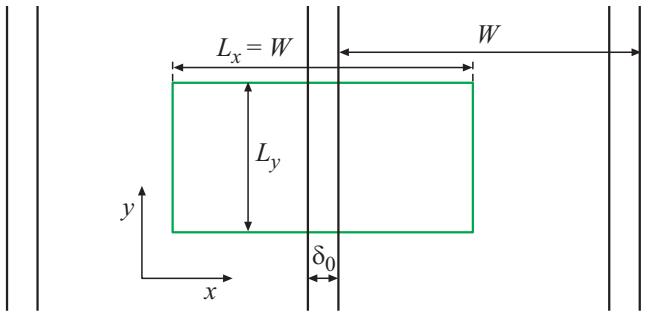

Figure 2. Schematic image of the OKMC model to calculate the sink strength of flat grain boundaries with width δ_0, separating grains with width W. Rectangle is the simulation cell. All beyond the calculation cell is the image formed by PBC.

where $\rho = \sqrt{\pi} r_0/L$, $L = L_x = L_y$. The next expression has the necessary properties:

$$\xi_0^{\pm}(L_x, L_y, r_0) = 12\frac{L_y}{L_x} \times \left(1 + \frac{6}{\pi}\frac{L_y}{L_x}\left(\ln\frac{L_y}{\sqrt{\pi} r_0} - \frac{3}{4} - \frac{\pi}{6} + \frac{c^{\pm}}{r_0}\right)\right)^{-1}, \tag{8}$$

in which, to further accuracy increasing of the description of the calculated data, a term $c^{\pm}/r_0$ was added, where indices „+“ and „−“ are used for SIAs and vacancies, respectively, $c^+ = 0.37a$, $c^- = 0.32a$. Eq. (8) describes OKMC data in Table 4 with minimum accuracy 0.6%.

5. Analytical expressions for sink strengths of LATBs considering interaction of LATBs with SPDs

The sink strength of a flat boundary (Figure 2), not interacting with SPD, has form of Eq. (3), where δ_0 is the boundary thickness. If absorbing surface is a set of cylindrical surfaces, not plain (Figure 1), then let's determine the effective thickness of the LATB $\delta_0^{\pm}$ as

$$\delta_0^{\pm} = L_x - \left(12 L_x L_y (1 + f_V)/\xi_0^{\pm}\right)^{1/2}, \tag{9}$$

where $\xi_0^{\pm}$ are either values taken from Table 4, or calculated according to Eq. (8).

Similarly to Eq. (9), for interacting LATBs we determine

$$\delta^{\pm} = L_x - \left(12 L_x L_y (1 + f_V)/\xi^{\pm}\right)^{1/2}. \tag{10}$$

Then the effect of interaction of LATBs with SPDs can be characterized by the value of increase in the effective thickness of the boundary when considering such interaction:

$$\zeta^{\pm} = \delta^{\pm} - \delta_0^{\pm} = \sqrt{12 L_x L_y (1 + f_V)}\left(\frac{1}{\sqrt{\xi_0^{\pm}}} - \frac{1}{\sqrt{\xi^{\pm}}}\right). \tag{11}$$

Table 4. Sink efficiencies of LATB dislocations not considering interactions between SPDs and LATBs in a BCC-crystal

Θ	T, K	$L_x = 150a$		$L_x = 300a$		$L_x = 600a$		$L_x = 900a$	
		ξ_0^+	ξ_0^-	ξ_0^+	ξ_0^-	ξ_0^+	ξ_0^-	ξ_0^+	ξ_0^-
0.75°	1	–	–	1.233	1.245	–	–	–	–
	2	–	–	1.497	1.503	–	–	–	–
	3	2.470	2.476	1.682	1.687	1.028	1.030	0.740	0.740
	6	–	–	2.100	2.101	–	–	–	–
	10	–	–	2.542	2.546	–	–	–	–
1.5°	1	1.428	1.444	0.926	0.933	0.545	0.547	0.385	0.387
	2	–	–	1.068	1.070	–	–	–	–
	3	2.063	2.071	1.158	1.160	0.617	0.619	0.421	0.421
	6	–	–	1.342	1.343	–	–	–	–
	10	–	–	1.516	1.517	–	–	–	–
3.0°	1	–	–	0.579	0.581	–	–	–	–
	2	–	–	0.631	0.632	–	–	–	–
	3	1.327	1.327	0.663	0.663	0.331	0.331	0.2205	0.2205
	6	–	–	0.722	0.722	–	–	–	–
5.0°	1	–	–	0.380	0.381	–	–	–	–
	2	–	–	0.402	0.402	–	–	–	–
	3	0.860	0.858	0.414	0.415	0.2036	0.2040	0.1348	0.1349
10°	1	–	–	0.1990	0.1994	–	–	–	–
	2	–	–	0.2054	0.2055	–	–	–	–
	3	0.441	0.441	0.2101	0.2099	0.1023	0.1026	0.0678	0.0678

Values $\xi^{\pm}$, obtained using Eq. (11) and OKMC-data from Table 1, 2 and 4 are well described by the approximating analytical dependence

$$\xi^{\pm}(L_x, L_y, T) = (L_y + p^{\pm})\left(1 - \frac{L_y}{2L_x}\right) \times \left(\frac{q^{\pm}}{L_y} - s^{\pm} \ln \frac{T}{T_1^{\pm}} + \frac{T}{T_2^{\pm}}\right), \quad (12)$$

where $p^{\pm}$, $q^{\pm}$, $s^{\pm}$, $T_1^{\pm}$, $T_2^{\pm}$ are parameters listed in Table 5.

So, from Eqs. (10), (11) and considering that $f_V = \pi r_0^2/(L_x L_y)$, for the value $\xi^{\pm}$ the analytical expression follows

$$\xi^{\pm}(L_x, L_y, T) = 12 \frac{L_x L_y + \pi r_0^2}{\left(L_x - \xi^{\pm}(L_x, L_y, T) - \delta_0^{\pm}(L_x, L_y, r_0)\right)^2}, \quad (13)$$

where $\delta_0^{\pm}(L_x, L_y, r_0)$ is determined by Eq. (9), $\xi^{\pm}(L_x, L_y, T)$ is determined by Eq. (12), $r_0 = 3a$. Analytically calculated values $\xi^{\pm}$ agree with OKMC data (Table 1, 2) within 1%. As an example, Figure 3 presents results of OKMC calculations and analytical calculations of ξ^+ using Eq. (13) at $L_x = 150a$ for Fe.

Analytical expression for LATB bias factor, following its definition (cl. 3) and Eq. (13), is written as follows

$$D(L_x, L_y.T) = 1 - \frac{\xi^-(L_x, L_y, T)}{\xi^+(L_x, L_y, T)} = 1 - \left(\frac{L_x - \xi^+(L_x, L_y, T) - \delta_0^+(L_x, L_y, r_0)}{L_x - \xi^-(L_x, L_y, T) - \delta_0^-(L_x, L_y, r_0)}\right)^2. \quad (14)$$

Eq. (14) describes the OKMC data (Table 3) well under all discussed combinations of parameters L_x, L_y, T. Figure 4 shows, as an example, a comparison of the OKMC data with analytical expression (14) at $L_x = 150a$.

In the studied ranges of parameters, $\delta_0^+ \approx \delta_0^-$ and $L_x \gg \delta^-$. So, Eq. (14) can be simplified

$$D(L_x, L_y, T) \approx \frac{\Delta\xi(L_x, L_y, T)}{L_x}\left(2 - \frac{\Delta\xi(L_x, L_y, T)}{L_x}\right), \quad (15)$$

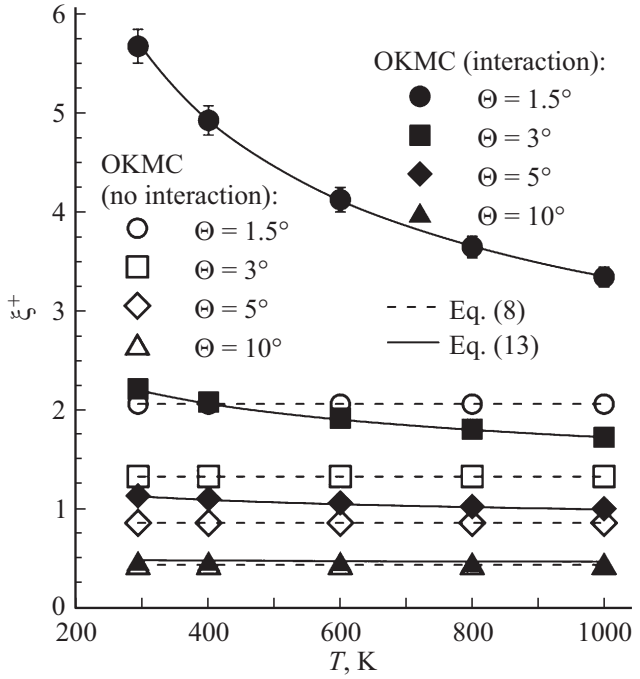

Figure 3. Temperature dependences of sink efficiencies of LATB dislocations for SIAs ξ^+ in Fe at the distance between neigbouring LATBs $L_x = 150a$. Dark and light symbols are the OKMC data considering and not considering interaction between LATBs and SPDs, respectively. Solid and dashed lines are calculations using Eqs. (13) and (8), respectively.

where

$$\Delta\xi(L_x, L_y, T) = \xi^+(L_x, L_y, T) - \xi^-(L_x, L_y, T),$$

$\xi^{\pm}(L_x, L_y, T)$ are determined by Eq. (12).

Table 5. Values of parameters of Eq. (12) for BCC metals Fe and V

Parameters	Fe		V	
	SIA (+)	Vacancy (−)	SIA (+)	Vacancy (−)
$p^{\pm}$, a	−2.747	1.359	−3.304	−3.380
$s^{\pm}$	0.9479	0.9833	0.7835	1.141
$T_1^{\pm}$, K	3984	538.4	3197	731.8
$T_2^{\pm}$, K	∞	1297	∞	1526
$q^{\pm}$, a	1.896	0	−3.369	0

6. Discussion

Let's consider the reason for the large difference in values of the LATB bias factor in Fe and V (Table 3, Figure 4). For this as a value characterizing interaction between LATBs and SPDs we take the maximum difference between energies of SPD migration in different directions ΔE. If a SPD is trapped by a LATB, when ΔE exceeds some value Q, then difference of distances $\Delta x_Q = x_Q^+ - x_Q^-$, at which $\Delta E^{\pm} = Q$ for SIAs (+) and vacancies (−), will correspond as per physical sence to the value $\Delta\xi$, and, as a consequence of Eq. (15), $\Delta x_Q \sim D$. The value of ΔE decreases with increasing x almost exponentially at $x > h$, at that the exponent in absolute value for V crystal is almost twice as much as for Fe crystal, due to the larger deviation of the elastic anisotropy factor $A = 2c_{44}/(c_{11} - c_{12})$ in Fe from unity ($A = 2.3$ for Fe, $A = 0.81$ for V, $A = 1$ in isotropic case) [7]. Ratio of values $\Delta E^+(x)/\Delta E^-(x) \approx 3$ for $x > h$ both for Fe, and for V. However, due to the

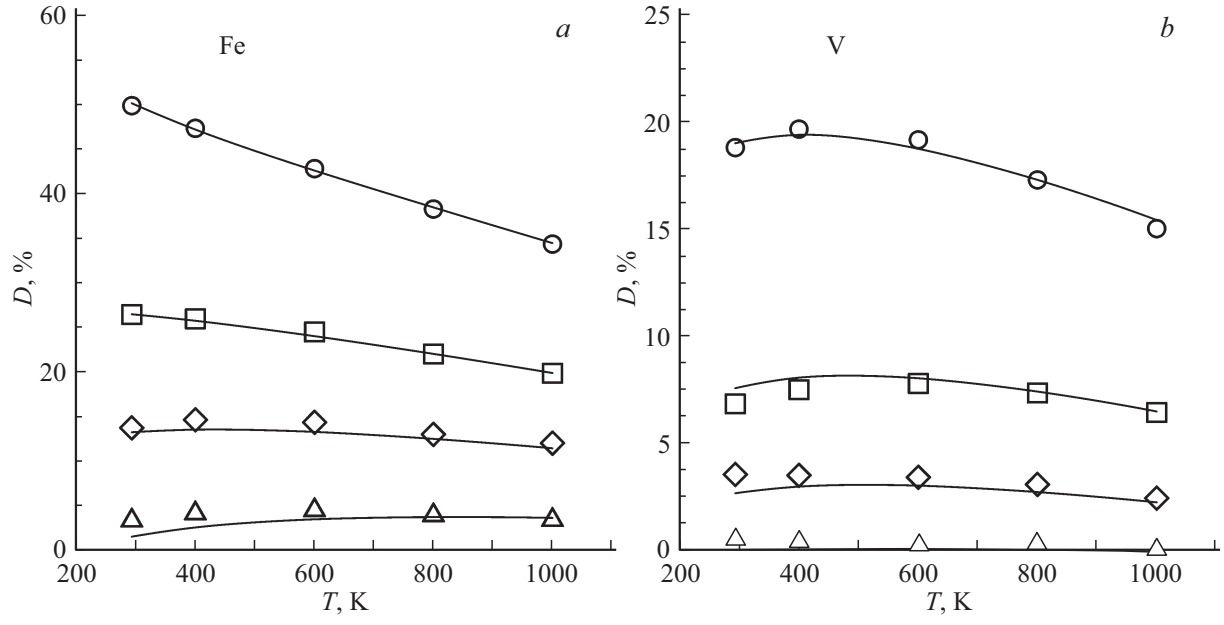

Figure 4. Temperature dependences of LATB bias factor D in Fe (a) and V (b) at the distance between neighbouring LATBs $L_x = 150a$. Symbols are the OKMC data. Solid lines are calculations using Eq. (14).

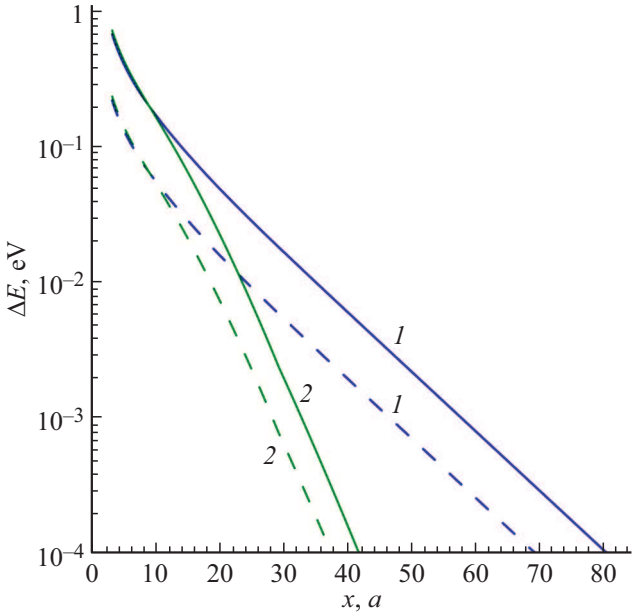

Figure 5. Maximum difference between energies of SPD migrations in different directions ΔE vs. distance x to LATB $\langle 111\rangle\{110\}$ with period $h = 30a$ ($\Theta = 1.65°$) in Fe (curves *1*) and V (curves *2*). Solid curves are for SIAs, dashed ones are for vacancies.

different exponents for Fe and V, the difference in distances differs significantly (by several times). For example, for $Q = 0.001$ eV, values Δx_Q for the LATB with $h = 30a$ ($\Theta = 1.65°$) are equal to $11.2a$ and $4.5a$ for Fe and V respectively (Figure 5), their ratio is ~ 2.5 times. For other LATBs, considered in this study, the value of this ratio is approximately same, this agrees with same ratio for values of the bias factor of the given LATB in Fe and V (Figure 4). Thus, high elastic anisotropy of Fe results in that values of bias factor of considered LATB dislocations are 2–4 times higher than the corresponding values for V.

High values of dislocation bias factor contribute to the nucleation and evolution of porosity in metals. Thus, polygonization of grains, as a result of which the edge dislocations are collected into low-angle tilt boundaries, significantly (by several times) reduces their bias factor, which helps to increase the material microstructure radiation resistance. It is possible to form a polygonal structure by appropriate thermomechanical treatments [15,16].

7. Conclusion

1. For low-angle tilt boundaries (LATBs) formed by dislocation walls from straight edge dislocations in slip systems $\langle 111\rangle\{110\}$ and $\langle 111\rangle\{112\}$, in BCC metals Fe and V, the sink strengths and bias factors for self-point defects are calculated by the object kinetic Monte Carlo method:

a) the sink strengths do not depend on the slip system of dislocations forming LATB within calculation accuracy;

b) the bias factor changes with temperature within 15–30% in the range 293–1000 K;

c) the bias factor is inversely proportional to the subgrain misorientation angle and the subgrain size;

d) the LATB bias factor is significantly (several times) less for V than for Fe (due to higher elastic anisotropy of Fe compared to V).

2. Approximating analytical expressions are obtained for the sink strengths and bias factors of LATBs in BCC metals Fe and V.

3. LATBs have a significantly lower bias factor than dislocations uniformly distributed over the bulk. LATB formation in metals (polygonization) increases their radiation resistance.

Funding

The study was carried out within the framework of the State Assignment of the National Research Center „Kurchatov Institute“ using computing resources of the federal collective usage center Complex for Simulation and Data Processing for Mega-science Facilities at NRC „Kurchatov Institute“ http://ckp.nrcki.ru/.

Conflict of interest

The authors declare that they have no conflict of interest.

References

[1] Elastic strain fields and dislocation mobility / Eds V.L. Indenbom, J. Lothe. Elsevier Science, North-Holland, Amsterdam (1992). 793 p.
[2] J. Hirth, J. Lothe. Theory of dislocations. John Wiley & Sons, Hoboken (1982). 857 p.
[3] R.W. Siegel, S.M. Chang, R.W. Balluffi. Acta Metall **28**, *3*, 249 (1980). https://doi.org/10.1016/0001-6160(80)90159-5
[4] A.H. King, D.A. Smiths. Rad. Eff. **54**, *3–4*, 169 (1981). https://doi.org/10.1080/00337578108210044
[5] R.R. Galimov, S.B. Goryachev. Phys. Status Solidi B **153**, *2*, 443 (1989). https://doi.org/10.1002/pssb.2221530204
[6] C. Jiang, N. Swaminathan, J. Deng, D. Morgan, I. Szlufarska. Mater. Res. Lett. **2**, *2*, 100 (2014). https://doi.org/10.1080/21663831.2013.871588
[7] A.B. Sivak, P.A. Sivak, V.A. Romanov, V.M. Chernov. PAS&T. Ser. Thermonuclear fusion **38**, *2*, 43–50 (2015). (in Russian) https://doi.org/10.21517/0202-3822-2015-38-2-43-50
[8] A.B. Sivak, V.A. Romanov, V.M. Chernov. Crystallography Rep. **55**, *1*, 97 (2010). https://doi.org/10.1134/S1063774510010153
[9] A.B. Sivak, V.M. Chernov, V.A. Romanov, P.A. Sivak. J. Nucl. Mater. **417**, *1–3*, 1067 (2011). https://doi.org/10.1016/j.jnucmat.2010.12.176
[10] A.B. Sivak, P.A. Sivak, V.A. Romanov, V.M. Chernov. Inorg. Mater. Appl. Res. **6**, *2*, 105 (2015). https://doi.org/10.1134/S2075113315020161 https://elibrary.ru/item.asp?id=22027294
[11] J.A. Rayne, B.S. Chandrasekhar. Phys. Rev. **122**, *6*, 1714 (1961). https://doi.org/10.1103/PhysRev.122.1714

[12] D.I. Bolef, R.E. Smith, J.G. Miller. Phys. Rev. B **3**, *12–15*, 4100 (1971). https://doi.org/10.1103/PhysRevB.3.4100
[13] S.I. Golubov, A.V. Barashev, R.E. Stoller. In: Comprehensive Nuclear Materials / Eds R.J.M. Konings, R.E. Stoller. 2 Ed. Elsevier, Amsterdam (2020). V. 1. P. 717. https://doi.org/10.1016/B978-0-12-803581-8.00663-9
[14] F.A. Nichols. J. Nucl. Mater. **75**, *1*, 32 (1978). https://doi.org/10.1016/0022-3115(78)90026-0
[15] T.N. Vershinina, Yu.R. Kolobov, M.V. Leont'eva-Smirnova. Steel in Translation **42**, *8*, 627 (2012). https://doi.org/10.3103/S0967091212080141
[16] T. Vershinina, M. Leont'eva-Smirnova. Mater. Characterization **125**, 23 (2017). https://doi.org/10.1016/j.matchar.2017.01.018

Translated by I.Mazurov